Robust Iteration-dependent Least Mean Square-based Distribution Static Compensator Using Optimized PI Gains*

*Sabha Raj Arya**, *Rakesh Maurya and Jayadeep Srikakolapu*
(Department of Electrical Engineering, Sardar Vallabhbhai National Institute of Technology, Surat 395007, India)

Abstract: A robust iteration-dependent least mean square (RIDLMS) algorithm-based fundamental extractor is developed to estimate the fundamental components of the load current for a four-wire DSTATCOM with a nonlinear load. The averaging parameter for calculating the variable step size is iteration dependent and uses variable tuning parameters. Rather than using the current value, the previous learning rate was used in this method to achieve a more adaptive solution. This additional control factor aids in determining the exact learning rate, resulting in reliable and convergent outcomes. Its faster convergence rate and the avoidance of local minima make it advantageous. The estimation of the PI controller gains is achieved through a self-adaptive multi-population algorithm. The adaptive change in the group number will increase exploration and exploitation. The self-adaptive nature of the algorithm was used to determine the subpopulation number needed according to the fitness value. The main advantage of this self-adaptive nature is the multi-population spread throughout the search space for a better optimal solution. The estimated gains of the PI controllers are used for the DC bus and AC terminal voltage error minimization. The RIDLMS-based control with PI gains obtained using the proposed optimization algorithm showed better power quality performance. The considered RIDLMS-supported control was demonstrated experimentally using d-SPACE-1104.

Keywords: Least mean square, variable learning, DSTATCOM, local minima, Rao algorithm, reactive power, neutral current

1 Introduction

Presently, for compactness, efficient energy utilization, and reliability, power electronics have encompassed nonlinear loads [1]. The nonlinear loads are responsible for the generation of harmonics; this causes the AC mains to deliver more reactive current, causing distortion of the voltage at the load and an increase in losses [2]. To mitigate this, active power conditioners are used in single-phase and three-phase arrangements [3]. The type of disability in power quality determines the type of connection with the AC mains [4]. Current harmonics and reactive power compensation require active line compensation to improve the current-based distortions [5]. The shunt active power filter can be operated in power factor and zero voltage regulation modes to mitigate current-based distortions [6]. DSTATCOM is a shunt active power filter whose performance relies on the control technique employed for gate signal pulse generation [7]. Many power system applications have been developed for the real-time governing of power systems; therefore, AC mains data is needed. Non-linear loads cause harmonic disturbances in the AC mains, which can be diagnosed using AC mains data. The AC mains data is collected using various methods such as state observer-based [8], zero-crossing detection [9], artificial neural networks [10], adaptive notch filters [11], phase-locked loops (PLL) [12], and least mean square estimation. The fractional part of a method for updating the LMS ingredients was presented in Ref. [13] with a lower mathematical burden. The convergence study of the sequential partial update LMS algorithm (S-LMS) with various assumptions can avoid divergence by recursively updating the coefficient. A two-step

Manuscript received March 30, 2021; revised May 30, 2021; accepted August 11, 2021. Date of publication December 31, 2022; date of current version December 30, 2021.
* Corresponding Author, E-mail: sabharaj79@gmail.com
* Supported by Science and Engineering Research Board -New Delhi Project (Extra Mural Research Funding Scheme), Grant No. SB/S3/EECE/030/2016.
Digital Object Identifier: 10.23919/CJEE.2022.000040

least-mean-square (LMS)-type adaptive algorithm was proposed by the authors in Ref. [14]. In this study, a non-stationary modified two-step LMS was considered to provide stable performance with better tracking performance during convergence. The extracted weight vector with increments was used as the weight vector for the next iteration.

A robust novel normalized least mean square (NLMS) was presented in Ref. [15], in which filter parameters dynamically regulate the internal variables. It is a developed gradient-descent type scheme. Methods based on convolution and cross-correlation techniques were introduced by Das et al. [16-17]. A fast robust recursive least squares (FRRLS) algorithm with a new arrangement in the control was introduced in Refs. [18-19]. These methods provide convergence and stable operation at the cost of the computational burden. A time-dependent constraint considering the norm update instead of the cost optimization function is given in Ref. [20]. A theoretical and experimental validation of the adaptive linear sinusoidal tracer control in Ref. [21] was provided. This algorithm was projected on a three-phase distribution system. A novel technique, LMS, was introduced in Ref. [22], which avoids the adaptive noise cancellation (ANC) problem. Because it depends on the squared Euclidian norm minimization of the weight vector with a stability constraint defining a posteriori estimation error. An adaptive LLMS was proposed in Ref. [23]; here, two LMS segments were connected in series, and the convergence process was performed using the mean square error. An adaptive algorithm was recognized using a robust step-size LMS algorithm. The variable step-size uses the weighted running average of the squared error signal [24]. Generally, many optimization techniques have control parameters that are algorithm-specific . In addition to this population size, the number of iterations is a factor that can control the optimization process. Control parameters should be tuned for a few algorithms, such as the artificial bee colony, particle swarm optimization, and harmony search algorithm. Similarly, other algorithms have their own algorithm-specific parameters. The appropriate tuning of control parameters sometimes negatively affects the optimization process [25-26]. Because of this, a new type of algorithm, which is an algorithm-specific parameter less Rao algorithm, is introduced [27]. The multi-population search process in advanced optimization enhances the optimization process. The total population is separated into a few groups in the multi-population search and is provided with the total search space to improve the diversity of the search process. The divide and combine strategy is used for communication among subpopulations. Ant-lion optimization has a better solution than existing fixed optimization problems [28]. Self-adaptive multi-population Rao (SAMP Rao) algorithms have been introduced by utilizing the advantages of Rao algorithms by integrating a multi-population approach. To regulate the exploration and exploitation rates in the searching procedure, SAMP Rao algorithms alter the group number adaptively according to the change in the best fitness value [29].

In this study, a recognized robust iteration-dependent LMS-based (RIDLMS) control algorithm is anticipated to control the DSTATCOM system. It is an improved control of the benchmark LMS that utilizes the previous learning rate to obtain a better adaptive solution rather than using the present value. The additional control factor assists in determining the exact quantity of the learning rate, which provides accurate and convergent results. Its faster convergence rate and the avoidance of local minima make it advantageous. The novelty of LMS is the iteration-dependent averaging parameter. These advantages over traditional LMS attracted authors to choose the RIDLMS-based control algorithm in the recognized DSTATCOM. By extracting the fundamental components from the unhealthy load current using this adaptive technology, the control algorithm can compensate for power quality problems. A delta ZigZag transformer is considered for neutral current compensation at the point of common coupling. The search process of the optimal solution evolution in the SAMP Rao algorithms is based on the best and worst results in the total population and arbitrary communication between populations. The SAMP Rao algorithms can solve computationally expensive design problems. The tuning of the PI gains was carried out using SAMP Rao algorithms owing to its multi-population advancement. This study provides meticulous details of the RIDLMS algorithm, along

with the operating principle. The recognized LMS technique for the system was supported by the simulation results and experimental verification using a laboratory setup.

2 System structure

The structure of the three-phase four-wire system with an AC voltage controller type nonlinear load and a DSTATCOM is shown in Fig. 1. A voltage source converter is made with six IGBT switches, and a DC bus capacitor is provided in the shunt to the system. The grid and load currents are i_G and i_L, respectively. Both currents will be unhealthy until compensator currents (i_C) from the DSTATCOM are introduced at the point of common coupling (PCC).

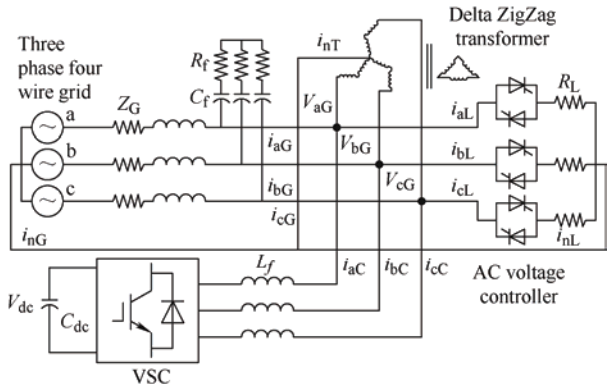

Fig. 1 System structure with AC voltage controller load and DSTATCOM

A proper and controlled operation of DSTATCOM can make the grid currents healthy and free from harmonics caused by the nonlinear load. In performing such operations, an interfacing inductance (L_f) and ripple filter (R_f and C_f) at the PCC are introduced. The grid impedance (ZG) was considered for the grid. A delta zigzag transformer was used for the neutral current compensation. The RIDLMS-based adaptive technique was inserted in the control scheme. The voltages and currents needed for the control schematic shown in Fig. 2 are sensed and processed in the control algorithm to generate the gate pulses for operating the DSTATCOM.

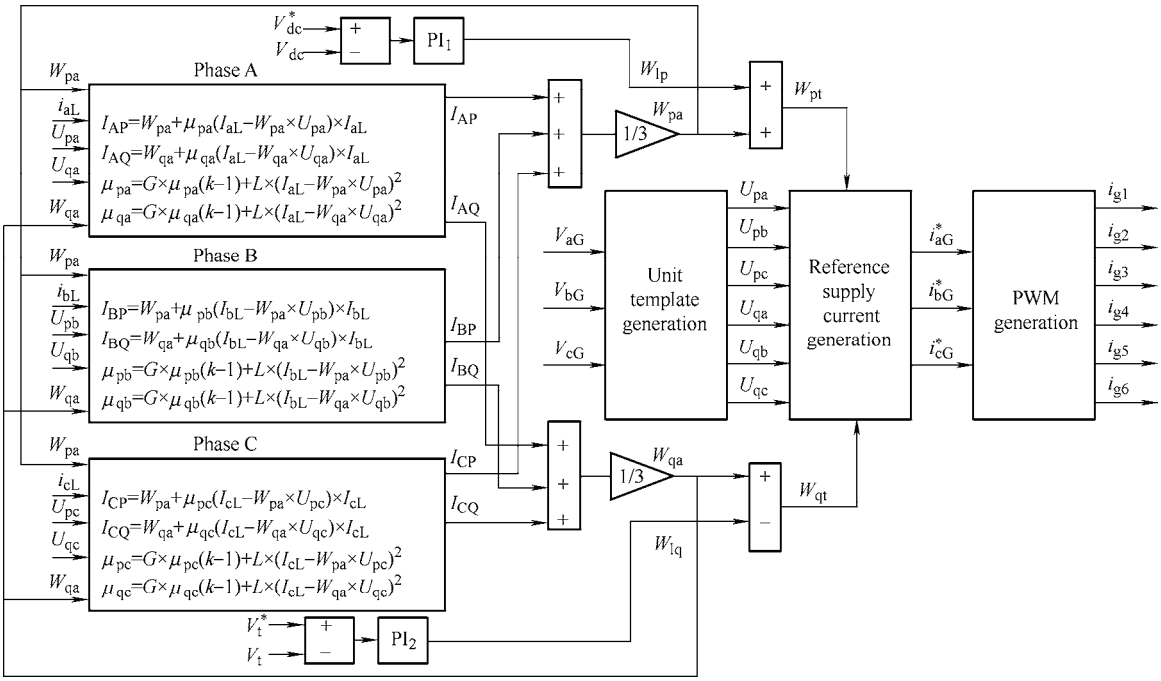

Fig. 2 Control algorithm of DSTATCOM using RIDLMS based control

3 Control techniques

The system structure provided in Fig. 1 was controlled using a control algorithm based on RIDLMS. This is illustrated in Fig. 2. Three-phase unhealthy load currents (i_L), grid currents (i_G), and DC bus voltage (V_{dc}) are collected online using Hall effect sensors. The adaptive algorithm, based on RIDLMS for fundamental component mining, is used in the control technique shown below. PI1 in the PFC method regulates the DC bus voltage. PI2 in the ZVR method regulates the AC terminal voltage. The harmonic load

current is fed through RIDLMS for each phase, and it provides in-phase and quadrature components of all three phases (IAP, IAQ, IBP, IBQ, ICP and ICQ). An average quantity is obtained from the in-phase and quadrature quantities, that is, W_{pa} and W_{qa}. These average quantities are fed back to the RIDLMS and used in fundamental extraction. The PI1 controller is fed with a DC bus voltage error and gives a loss component W_{lp} in the PFC mode, whereas the PI2 controller is fed with a terminal voltage error and gives a loss component W_{lq} in the ZVR mode. These loss components are added up with the average quantity and subtracted from the average quantity for in-phase and quadrature quantities, respectively, to obtain the total quantities W_{pt} and W_{qt}. These total quantities are multiplied by unit templates to generate reference grid currents. The error current obtained by comparing the actual and reference grid currents was used for generating gate pulses for DSTATCOM through sinusoidal PWM switching.

3.1 Estimation of voltage unit templates

The grid voltages (V_{ph}) at the PCC and terminal voltage (V_t) were calculated using the following equation [2, 20]

$$V_t = \sqrt{\frac{2\left(V_{aG}^2 + V_{bG}^2 + V_{cG}^2\right)}{3}} \tag{1}$$

The unit vectors U_{pa}, U_{pb}, and U_{pc} and its quadrature unit vectors U_{qa}, U_{qb}, and U_{qc} are estimated [2, 3, 20].

3.2 Control scheme based on RIDLMS for DSTATCOM

The nonlinear reference signal generation for DSTATCOM depends primarily on the RIDLMS used for fundamental extraction in the control algorithm. The harmonic load current of each phase is fed through RIDLMS for the extraction of fundamental in-phase and quadrature quantities, i.e. I_{AP} and I_{AQ} of phase "a," I_{BP} and I_{BQ} of phase "b," and I_{CP} and I_{CQ} of phase "c". The LMS adaptive technique employed in Phase "a" is illustrated in Eqs. (3) and (4), and the same was employed for the remaining phases [24].

$$I_{AP} = W_{pa} + \mu_{pa}(I_{aL} - W_{pa} \times U_{pa}) \times I_{aL} \tag{2}$$

$$I_{AQ} = W_{qa} + \mu_{qa}(I_{aL} - W_{qa} \times U_{qa}) \times I_{aL} \tag{3}$$

The error quantity $e(k)$ is obtained by multiplying the difference between the load current I_{aL} and the product of the weight W_{pa} and unit template U_{pa}, as shown below

$$e(k) = I_{aL}(k) - W_{pa}(k) \times U_{pa}(k) \tag{4}$$

The Learning rate is calculated using iteration dependent constants "G," "L," and error "e". The learning rates for the recognized LMS are given as follows

$$\mu_{pa} = G \times \mu_{pa}(k-1) + L \times (I_{aL} - W_{pa} \times U_{pa})^2 \tag{5}$$

$$\mu_{qa} = G \times \mu_{qa}(k-1) + L \times (I_{aL} - W_{qa} \times U_{qa})^2 \tag{6}$$

$$G = ((1-i)/i) \times G_c \tag{7}$$

$$L = L_c / I \tag{8}$$

Constants G_c and L_c are 0.98 and 0.03, respectively [24].

Similarly, the P and Q components for the phase "b" and Phase "c" load currents were extracted.

3.3 Load current components estimation

The average in-phase load current component of all three phases was calculated, and it is termed the load active component (W_{pa}) [2, 20], written as

$$W_{pa} = (I_{AP} + I_{BP} + I_{CP})/3 \tag{9}$$

The average quadrature load current component of all three phases was calculated, and it is termed the load reactive component (W_{qa}), written as

$$W_{qa} = (I_{AQ} + I_{BQ} + I_{CQ})/3 \tag{10}$$

3.4 Production of gate pulses

The objective of PI controller PI_1 is to control the DC bus voltage, and the output of PI_1 provides W_{lp}. The objective of PI_2 is to control the grid terminal voltage, and the output of PI_2 provides W_{lq}. These quantities are added to the load current components to obtain the total active and reactive weights as follows [5, 9]

$$W_{pt}(k) = W_{lp}(k) + W_{pa}(k) \tag{11}$$

$$W_{qt}(k) = W_{qa}(k) - W_{lq}(k) \tag{12}$$

The unit templates and the obtained total weights aid in estimating the reference grid currents as follows

$$I_{aG}^* = U_{pa} \times W_{pt} + U_{qa} \times W_{qt} \tag{13}$$

$$I_{bG}^* = U_{pb} \times W_{pt} + U_{qb} \times W_{qt} \tag{14}$$

$$I_{cG}^{*} = U_{pc} \times W_{pt} + U_{qc} \times W_{qt} \quad (15)$$

The error currents obtained by subtracting the actual grid currents from their reference values were used for generating gate pulses that control the DSTATCOM.

3.5 Estimating controller gains using self-adaptive multi population (SAMP) Rao algorithm

Optimal gain estimation using the SAMP Rao algorithm with an optimization problem formulated with DC bus error minimization and AC terminal voltage error minimization is as follows: Evading all the worst solutions and moving near the best solution is the approach of the SAMP Rao algorithm for an optimization problem. A voltage regulation of 0.28% and number of iterations of 20 is the termination criterion in this optimization problem.

The designed variables are "y" varying in number from 1 to i. The Candidates are "m" varying in number from 1 to j. One candidate $f(g)$ attains a best solution value of $f(g)_{best}$, and another candidate $f(g)$ attains the worst solution value of $f(g)_{worst}$ at an iteration "x". The quantity of variables and the number of candidates decide the number of iterations [27, 29].

If $g_{y,z,x}$ is the value of the y^{th} variable for the z^{th} candidate during the x^{th} iteration, the following equation gives the modified value

$$g_{y,z,x}^{1} = g_{y,z,x} + r_1 \left(g_{y,best,x} - g_{y,worst,x} \right) \quad (16)$$

where $g_{y,best,x}$ represents the best candidate value of variable y for the x^{th} iteration, $g_{y,\,worst,\,x}$ represents the worst candidate value of variable y for the x^{th} iteration, $g_{y,z,x}^{1}$ represents the updated $g_{y,\,z,\,x}$, r_1 represents the random number for the best solution tendency closeness.

A better function value of $g_{y,z,x}^{1}$ is admitted and input to the next iteration and the random variable r_1 is between 0 and 1. The proposed method was illustrated using a flow chart, as shown in Fig. 3. The recognized SAMP Rao algorithms employ a number of subpopulations by grouping the total population into various groups based on the solution's worthiness. The multi population spread throughout the search space can provide a better optimal solution. The adaptive change in the number of groups increases the exploration and exploitation of the optimal solution search.

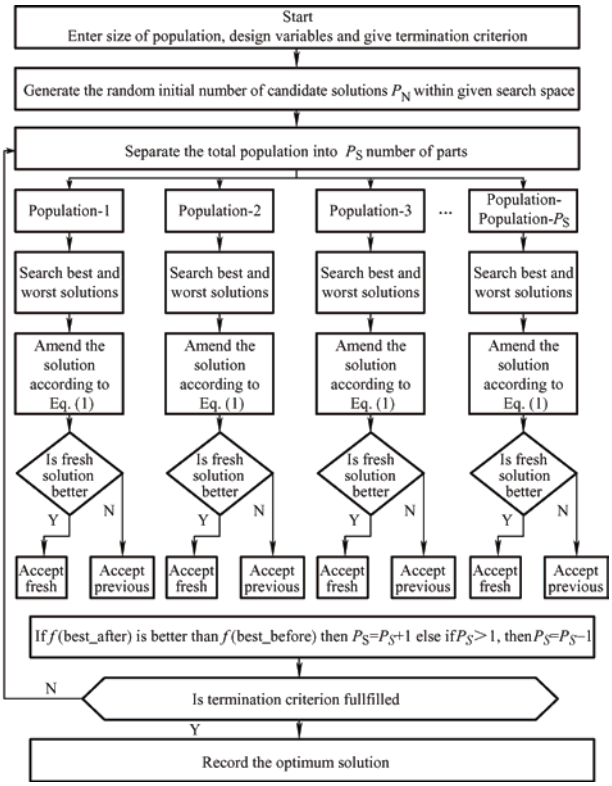

Fig. 3 Flowchart of SAMP Rao algorithms

4 Simulation results and discussion

The working of the recognized control for operating the DSTATCOM is shown with a simulation made in Matlab. The simulation was carried out using the parameters listed in Tab. 1. The simulation was conducted for 4 s by providing a dynamic load in the "a" phase and "c" phase from 3.1 s to 3.3 s.

The operating modes of the DSTATCOM were tested using the parameters considered. The performance of the system in these methods, namely the PFC and ZVR methods, is provided in the subsequent sections (Figs. 4-8). During the DSTATCOM operation in PFC mode, the performance of the SAMP Rao algorithm against the number of iterations is shown in Figs. 4a-4c. The cost function in the PFC mode of operation is shown in Fig. 4a, which settled at 4 549 in the 8th iteration. The proportional gain K_p of the DC PI is shown in Fig. 4b, and its optimized value is 0.5. The integral gain K_i of the DC PI is shown in Fig. 4c, and its optimized value is 0.1. The performance of the SAMP Rao algorithm with respect to the number of iterations during the DSTATCOM operation in ZVR mode is shown in Figs.

4d-4f. The cost function in the ZVR mode of operation is shown in Fig. 8d, which settled at 8 550 in the 8th iteration. The proportional gain K_p of the AC PI is shown in Fig. 4e, and its optimized value is 1.5. The integral gain K_i of the AC PI is shown in Fig. 4f, and its optimized value is 0.1. These optimized values maintained a DC bus voltage V_{dc} of 700 V and AC terminal voltage V_t of 339 V.

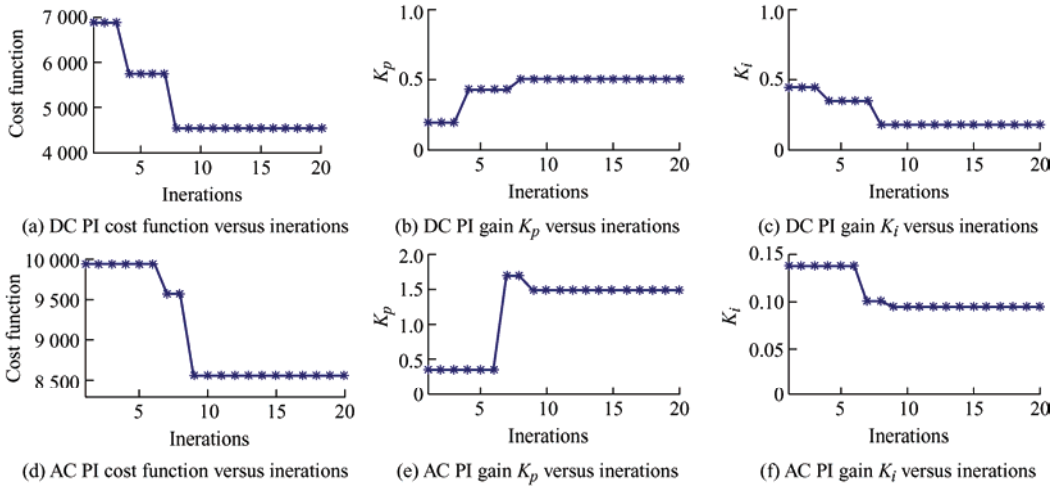

Fig. 4 Optimization analysis using Rao1 algorithm

Tab. 1 Parameters for simulation work

Parameter		Value
PCC voltage V_s		415 V, 50 Hz
Non-linear load		3-ϕ AC voltage controller with R=15 Ω
DC-link voltage V_{dc}/V		700
DC bus capacitor C_{dc}/μF		5 000
Grid impedance Z_G		R=0.1 Ω, L=2 mH
Converter interfacing inductance L_f/mH		3.25
RC filter	R_f/Ω	5
	C_f/μF	10
LPF cut off frequency/Hz		10
Switching frequency/kHz		2.5
Sampling time T_s/μs		20

4.1 Performance analysis of the internal signals of the control algorithm during load dynamics

The internal signals of the RIDLMS-based control used for mining the fundamental components are shown in Fig. 5.

The learning rates are μ_{pa} and μ_{qa}, average load active and load reactive components are w_{pa} and w_{qa}, PI_1 and PI_2 are w_{lp} and w_{lq}, controllers' output total active and reactive power components are w_{pt} and w_{qt}, and actual and reference grid currents of phase "a" are i_G and i_G^*. The actual grid current tracks the reference grid current even under dynamic load conditions, i.e., phase "a" removal at 3.1 sand phase "c" removal at 3.2 s. The response is quick and accurate, which helps in the proper extraction of fundamental components using RIDLMS.

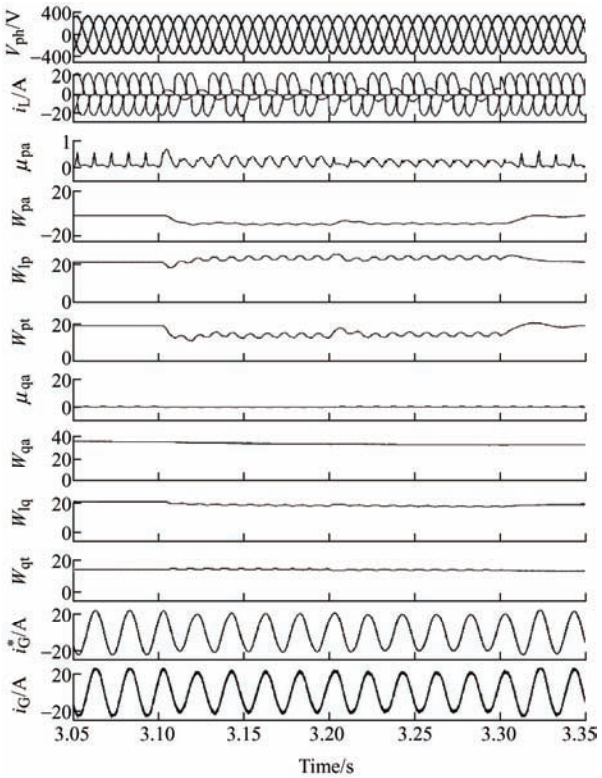

Fig. 5 Internal signals of the proposed control algorithm in ZVR mode

4.2 Response of DSTATCOM in PFC mode

The recognized RIDLMS-based control algorithm aids

the DSTATCOM for operation in PFC mode. Its performance was observed, as shown in Fig. 6. The grid phase voltage is V_{ph}; grid current is i_G; load currents are i_{aL}, i_{bL}, and i_{cL}; compensator currents are i_{aC}, i_{bC}, and i_{cC}; DC link voltage is V_{dc}; and terminal voltage is V_t. The dynamic load removal was carried from 3.1 s to 3.3 s. The performance was observed to be satisfactory, as the balancing of the load during dynamic load inclusion occurred at t=3.1 s, dynamic load removal occurred at t=3.2 s in phase "a," dynamic load inclusion occurred at t=3.2 s, and dynamic load removal occurred at t=3.3 s in phase "c" The grid currents were observed to be sinusoidal and balanced during the dynamic load conditions.

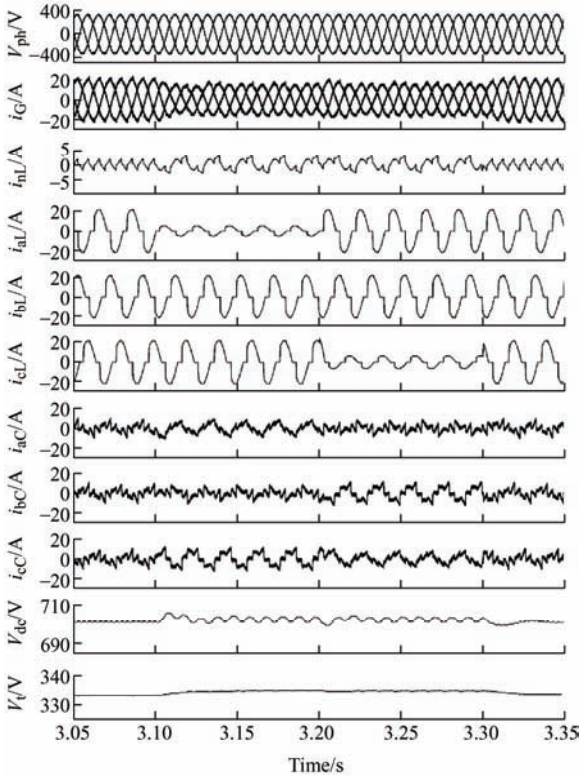

Fig. 6 System with nonlinear load in PFC mode with dynamic load variations

The grid current recovered in two fundamental cycles in both the inclusion and removal of the dynamic load. The function of DSTATCOM in mitigating the grid current harmonics and reactive power compensation has been achieved, and the power factor correction mode of operation is shown in the phase of grid current and grid voltage. Fig. 8a shows that the THD of the phase "a" voltage was found to be 2.81%, and Fig. 8b shows that the THD of the phase "a" grid current was found to be 4.51%, which was improved from a THD of 22.91% for the phase "a" load current, shown in Fig. 8c.

4.3 Performance of DSTATCOM in ZVR mode

The recognized RIDLMS-based control algorithm aids DSTATCOM operation in ZVR mode. Its performance was observed, as shown in Fig. 7. The grid phase voltage is V_{ph}; grid current is i_G; load currents are i_{aL}, i_{bL}, and i_{cL}; compensator currents are i_{aC}, i_{BC} and i_{cC} DC link voltage is V_{dc}; and terminal voltage is V_t. The dynamic load was carried from 3.1 s to 3.3 s.

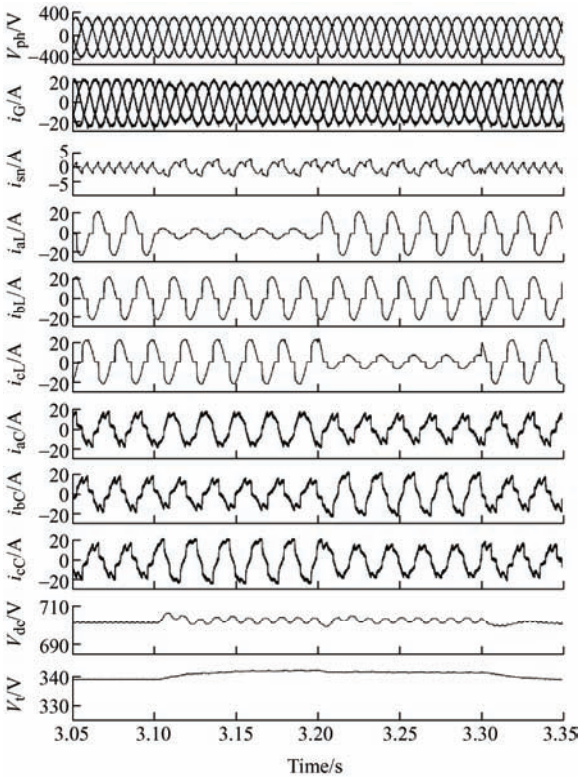

Fig. 7 System with nonlinear load in ZVR mode with dynamic load variations

The performance was observed to be satisfactory, as the balancing of the load during dynamic load inclusion occurred at t=3.1 s, dynamic load removal at time (t) equal to 3.2 s in phase "a" dynamic load inclusion at t=3.2 s, and dynamic load removal at time (t) equal 3.3 s in phase "c". The grid currents were observed to be sinusoidal and balanced during the dynamic load conditions. The grid current recovered in two fundamental cycles in both the inclusion and removal of the dynamic load. The function of the DSTATCOM in mitigating the grid current harmonics and reactive power compensation was demonstrated,

and the leading nature of the grid current and grid phase voltage showed the zero-voltage regulation mode of operation. Fig. 8d shows that the THD of the phase "a" voltage was found to be 3.16%, and Fig. 8e shows that the THD of the phase "a" grid current was found to be 4.81%, which was improved from a THD of 23.37% for the phase "a" load current, shown in Fig. 8f.The leading nature of the grid current with respect to the grid voltage proves the ZVR mode of operation of the DSTATCOM. The THD values of the grid parameters in the PFC and ZVR mode are shown in Fig. 6. The THD values of the grid voltage and grid currents are within the safe limits, which proves the capability of the DSTATCOM with the recognized control algorithm.

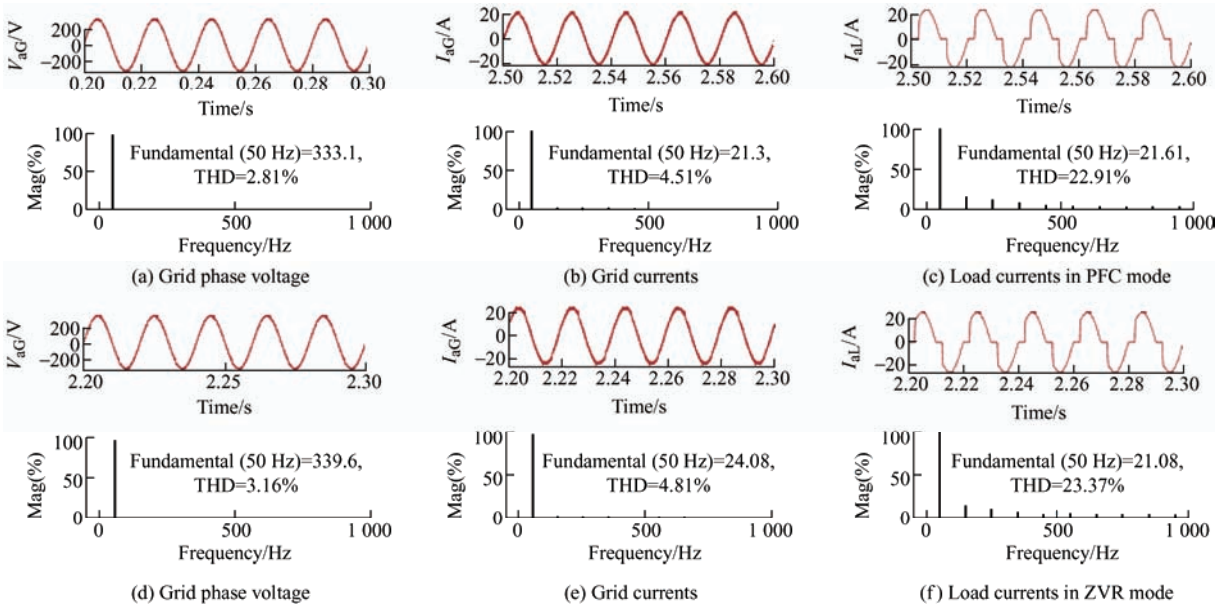

Fig. 8 THD analysis

5 Experimental validation

The robust iteration-dependent LMS control algorithm used in DSTATCOM was applied for real-time implementation. Grid currents, load currents, and PCC voltages were sensed using LEM-made Hall effect sensors. A DSP (d-SPACE-1104) controller was used to realize the recognized LMS controller for DSTATCOM with a sampling rate of 40 μs. An isolation circuit using an opto-coupler (IC6N136) and Transistor (TL2N2222) was used. A four-channel DSO was used to capture the dynamic performance of the system. A fluke-made power quality analyzer was used to analyze the THD under steady-state conditions. The parameters used for the hardware implementation are provided in Tab. 2. The laboratory setup using the d-SPACE-1104 is shown in Fig. 9.

Tab. 2 Parameters for experimental work

Parameter		Value
PCC voltage V_s/V		105 (50 Hz)
Non-linear load		3-ϕ AC voltage controller with R=21 Ω
DC-link voltage V_{dc}/V		200
DC bus capacitor C_{dc}/μF		5 000
Grid impedance Z_G		R=0.1 Ω, L=2 mH
Converter interfacing inductance L_f/mH		4
RC filter	R_f/Ω	5
	C_f/μF	10
LPF cut off frequency/Hz		10
Switching frequency/kHz		2
Sampling time T_s/μs		40

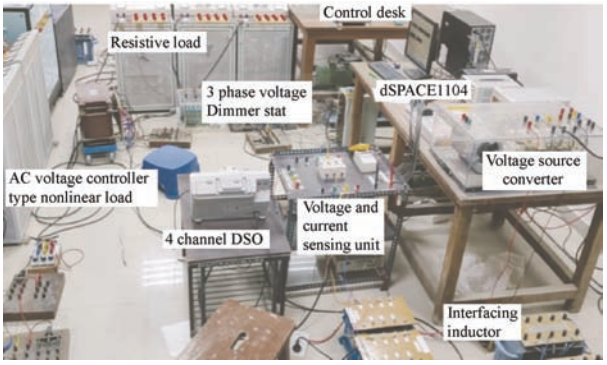

Fig. 9 Experimental setup developed in the laboratory using the d-SPACE-1104

The performance of the DSTATCOM is analyzed using RIDLMS using an AC voltage controller type nonlinear load in PFC mode, and the test results are as follows.

5.1 Dynamic performance of DSTATCOM system

An analysis of the system with the RIDLMS is shown in Fig. 10.

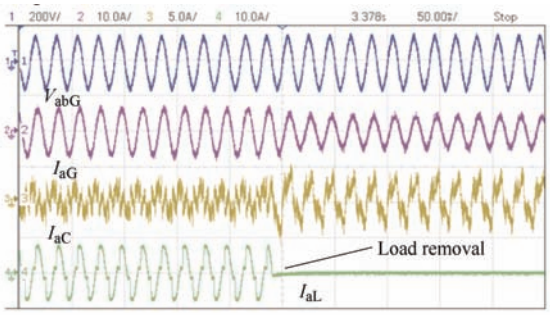

(a) Ch$_1$: V_{abG}; Ch$_2$: I_{aG}; Ch$_3$: I_{aL}; Ch$_4$: I_{aC}

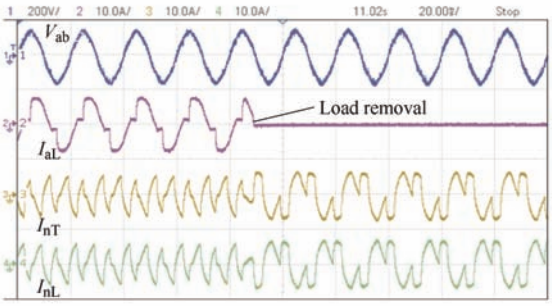

(b) Ch$_1$: V_{abG}; Ch$_2$: I_{aL}; Ch$_3$: I_{nT}; Ch$_4$: I_{nL}

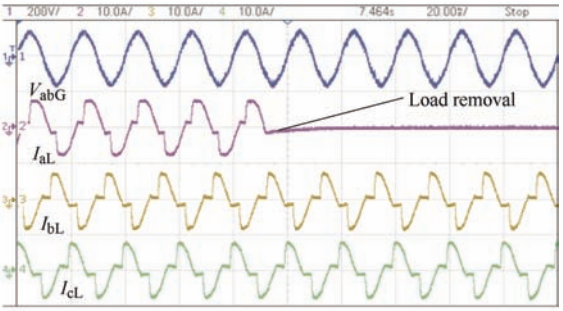

(c) Ch$_1$: V_{abG}; Ch$_2$: I_{aL}; Ch$_3$: I_{bL}; Ch$_4$: I_{cL}

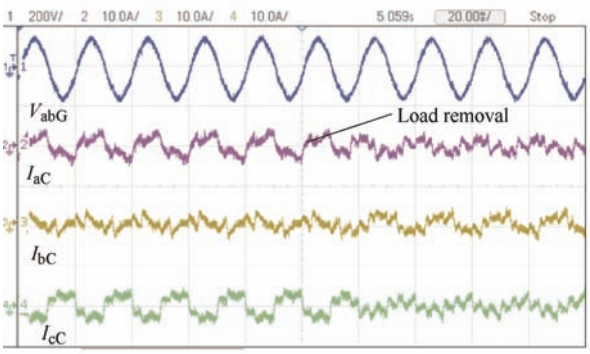

(d) Ch$_1$: V_{abG}; Ch$_2$: I_{aC}; Ch$_3$: I_{bC}; Ch$_4$: I_{cC}

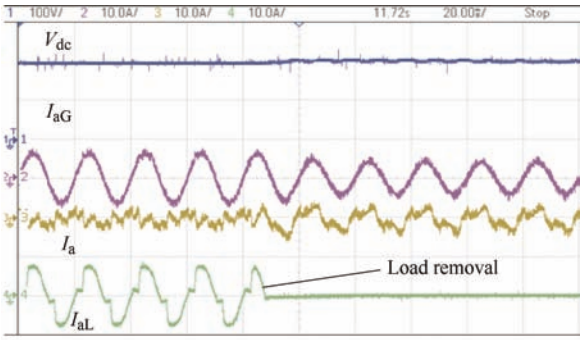

(e) Ch$_1$: V_{dc}; Ch$_2$: I_{aG}; Ch$_3$: I_{aC}; Ch$_4$: I_{aL}(20 ms/div)

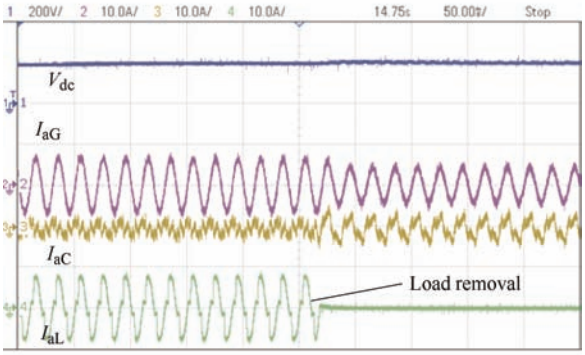

(f) Ch$_1$: V_{dc}; Ch$_2$: I_{aG}; Ch$_3$: I_{aC}; Ch$_4$: I_{aL}(50 ms/div)

Fig. 10 Dynamic performance of DSTATCOM during load removal condition

The grid currents, load currents, and compensator currents are sensed, along with the grid voltage (V_{abg}) and DC bus voltage (V_{dc}) during dynamic load removal in one phase. A dynamic load condition was created by removing a phase, followed by a regular load injection of 21 Ω. Fig. 10a shows the grid voltage, grid current, load current and compensator current. Similarly, Fig. 10b illustrates the load current I_{aL}, transformer neutral (I_{nT}) current, and load neutral current (I_{nL}), along with the grid voltage. It is evident that the neutral current compensation is performed successfully using the transformer. During the transition from dynamic phase removal to regular load inclusion, the variation in neutral current is detected.

Figs. 10c-10d illustrate the reaction of all load currents (I_{aL}, I_{bL}, and I_{cL}) and compensator currents (I_{aC}, I_{bC}, and I_{cC}), along with the grid voltage. The DC bus voltage is regained in less than three fundamental cycles. This is evident from Fig. 10e. The magnified version of Fig.10e, with higher time values, is shown in Fig. 10f. This matches the simulated results. These observations conclude that the dynamic condition of the system is satisfactory.

5.2 Steady-state performance of DSTATCOM

An illustration of the waveforms of the grid current (i_{ag}), load current (i_{aL}), and compensator current (i_{aC}), with respect to the grid voltage (V_{abg}) under steady state is shown in Figs. 11a-11c.

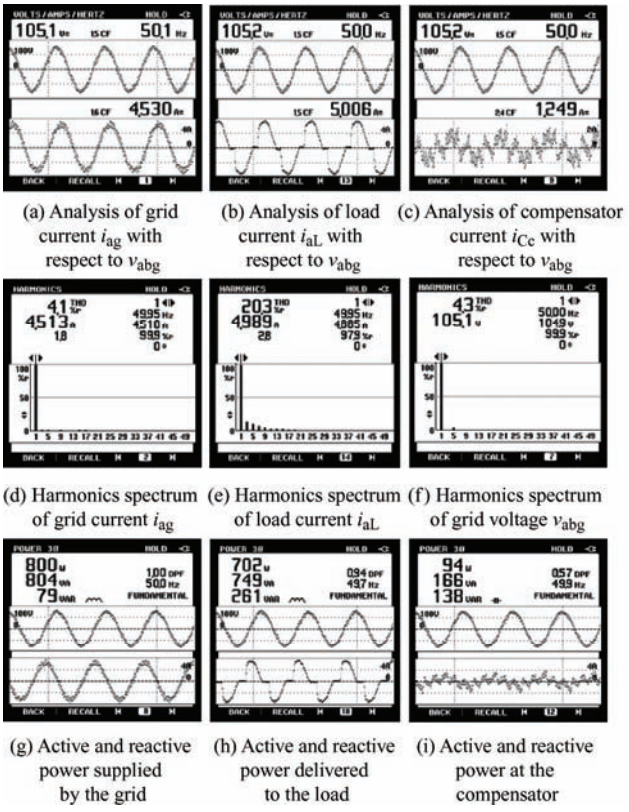

Fig. 11 Steady-state performance of DSTATCOM

The harmonic analysis of the grid current of phase "a" is shown in Fig. 11d, and the distortions are within an acceptable range. Fig. 11e shows the steady-state harmonic analysis of the phase "a" load current. Fig. 11f shows the steady-state harmonic analysis of the phase "a" voltage. It is observed that the harmonics of the grid current and grid voltage are 4.1% and 4.3%, respectively. The load harmonics were 20.3%. This demonstrates the acceptable functioning of DSTATCOM in the PFC mode of operation. The power factor at the AC mains is improved to unity after DSTATCOM compensates for the reactive power. Fig. 11g and show that the grid side has 79 Var and the load side has 261 Var. The reactive power supplied by the DSTATCOM was 138 Var. Fig. 11g shows the active power at the grid as 800 W and reactive power as 79 Var, Fig. 11h shows the active power at a load of 702 W and reactive power of 261 Var, and Fig. 11i shows the active power at the compensator as 94 W and reactive power as 138 Var. The nonlinear load considered here is an AC voltage controller with a resistive load. The amount of active power and reactive power before DSTATCOM compensation is 702 W and 261 Var, respectively, which is evident from the power analysis captured at the DSTATCOM. The grid drives the active power to the compensator and load. The compensator drives the reactive power to the load and the grid. This is proved by the unity displacement factor at the grid terminals. This verifies the acceptable operation of the system for the considered AC voltage controller-based nonlinear load.

6 Conclusions

In this study, a variable step size algorithm was used, in which the weight vector was updated with a varying step size. Iteration-dependent averaging parameters differ from RIDLMS in reducing the adaption time by taking a larger initial step size. Fundamental mining from a highly polluted load current using this new adaption theory of RIDLMS has exhibited better performance for DSTATCOM in all its operating modes. Grid abnormalities, such as phase imbalance and load current harmonics, have been observed and mitigated using the recognized least mean square adaptive algorithm. The stability, convergence, and robustness of the algorithm were achieved through the weighted variable step-size. RIDLMS produces synchronized fundamental signals with a constant amplitude despite a phase imbalance in the load current. The multi-population approach in the search process of the SAMP Rao algorithm to control exploration and exploitation has obtained optimized PI gains with eight iterations in both the PFC and ZVR modes. The performance of the RIDLMS-based

control algorithm for DSTATCOM was realized for performing laboratory trials with the help of d-SPACE-1104, which showed better performance.

References

[1] A M Munoz. Power quality: Mitigation technologies in a distributed environment. London: Springer-Verlag, 2007.

[2] S J Alam, S R Arya. Control of UPQC based on steady state linear Kalman filter for compensation of power quality problems. C*hinese Journal of Electrical Engineering*, 2020, 6(2): 52-65.

[3] A Martins, J Ferreira, H Azevedo. Power quality. Intech Press, 2011.

[4] G Benysek. Improvement in the quality of delivery of electrical energy using power electronics. London: Springer-Verlag, 2007.

[5] S G Basha, V Mani, S Mopidev. Single-phase thirteen-level dual-boost inverter based shunt active power filter control using resonant and fuzzy logic controllers. *IEEE-CSEE Journal of Power and Energy Systems*, DOI: 10.17775/CSEEJPES.2020.02640.

[6] G Rashed, H Haider, M.B. Shafik. Enhancing energy utilization efficiency of Pakistani system considering FACTS devices and distributed generation: Feasibility study. *Chinese Journal of Electrical Engineering*, 2020, 6(2): 66-82.

[7] A Emadi, A Nasiri, S B Bekiarov. Uninterruptible power supplies and active filters. New York: CRC Press, 2005.

[8] Hao Pan, Qingfang Teng, Dangdang Wu. MESO-based robustness voltage sliding mode control for AC islanded micro grid. *Chinese Journal of Electrical Engineering*, 2020, 6(2): 83-93.

[9] A Routray, A K Pradan, K P Rao. A novel Kalman filter for frequency estimation of distorted signals in power systems. *IEEE Transactions on Instrumentation Measurement*, 2002, 51(3): 469-479.

[10] R W Brug, F P Dawson, R Bonert. New synchronization method for thyristor power converters to weak AC systems. *IEEE Transactions on Industrial Electronics*, 1993, 40(5): 505-511.

[11] Xiaoli Yang, Zongshuai Hu, Rusen Fan, et al. Weighted least squares state estimation based on the optimal weight. *Proc. of Third International Conference on Technological Advances in Electrical, Electronics and Computer Engineering (TAEECE)*, 2015: 12-16.

[12] B Singh, J Solanki, V Varma. Neural network based control of reduced rating DSTATCOM. *in Proc. of Annual IEEE India Conference- Indicon*, 2005: 1830-1841.

[13] M Godavarti, A O Hero. Partial update LMS algorithms. *IEEE Transactions on Signal Processing*, 2005, 53(7): 2382-2399.

[14] A K Kohli, D K Mehra. Tracking of time-varying channels using two-step LMS-type adaptive algorithm. *IEEE Transactions on Signal Processing*, 2006, 54(7): 2606-2615.

[15] Y Choi, H Shin, W Song. Robust regularization for normalized LMS algorithms. *IEEE Transactions on Circuits and Systems-II*: *Express Briefs*, 2006, 53(8): 627-631.

[16] D P Das, S R Mohapatra, A Routray, et al. Filtered-s LMS algorithm for multichannel active control of nonlinear noise processes. *IEEE Transactions on Speech and Audio Processing*, 2006, 14(5): 1875-1880.

[17] D P Das, G Panda, S M Kuo. New block filtered-X LMS algorithms for active noise control systems. *IET Signal Processing*, 2007, 1(2): 73-81.

[18] L R Vega, H Rey, J Benesti, et al. A fast robust recursive least-squares algorithm. *IEEE Transactions on Signal Processing*, 2009, 57(3): 1209-1215.

[19] M Z A Bhotto, A Antoniou. Robust recursive least-squares adaptive-filtering algorithm for impulsive-noise environment. *IEEE Signal Processing Letter*, 2011, 18(3): 185-188.

[20] B Singh, S R Arya. Adaptive theory based improved linear sinusoidal tracer control algorithm for VSC. *IEEE Transactions on Power Electronics*, 2013, 28(8): 3768-3778.

[21] J B Foley, F M Boland. Comparison between steepest descent and LMS algorithms in adaptive filters. *IEE Proceedings*, 1987, 134(3): 283-289.

[22] J M Gorriz, J Ramírez, S Cruces-Alvarez, et al. A novel LMS algorithm applied to adaptive noise cancellation. *IEEE Signal Processing Letters*, 2009, 16(1): 34-37.

[23] J A Srar, K Chung, A Mansour. Adaptive array beam forming using a combined LMS-LMS algorithm. *IEEE Transactions on Antennas and Propagation*, 2010, 58(11): 3545-3557.

[24] U B Mansoor, S M Asad. A robust, iteration dependent variable step-size (RID-VSS) least-mean square (LMS) adaptive algorithm. *Proc. 2020 International Conference on Engineering and Emerging Technologies (ICEET)*, Lahore, Pakistan, 2020: 1-4.

[25] R T Marler, J S Arora. Survey of multi objective optimization methods for engineering. *Journal of Structural and Multidisciplinary Optimization*, 2004, 26(6): 369-395.

[26] K Amritha, V Rajagopal, K N Raju, et al. Ant lion

algorithm for optimized controller gains for power quality enrichment of off-grid wind power harnessing units. *Chinese Journal of Electrical Engineering*, 2020, 6(3): 85-97.

[27] R V Rao. Rao algorithms: Three metaphor less simple algorithms for solving optimization problems. *International Journal of Industrial Engineering Computations*, 2020(11): 107-130.

[28] Jiuzhong Zhang, Xueming Ding. A multi-swarm self-adaptive and cooperative particle swarm optimization. *Journal of Engineering Applications of Artificial Intelligence*, 2020, 24(6): 958-967.

[29] R V Rao, R B Pawar. Self-adaptive multi-population Rao algorithms for engineering design optimization. *Journal of Applied Artificial Intelligence*, 2020, 34(3): 187-250.

Sabha Raj Arya (M'12-SM'15) received Bachelor of Engineering degree in Electrical Engineering from Government Engineering College Jabalpur, in 2002, Master of Technology in Power Electronics from Motilal National Institute of Technology, Allahabad, in 2004 and Ph.D. degree in Electrical Engineering from Indian Institute of Technology (I.I.T) Delhi, New Delhi, India, in 2014. He is joined as Assistant Professor, Department of Electrical Engineering, Sardar Vallabhbhai National Institute of Technology, Surat. On January 2019, he was promoted as Associate Professor in same institute. His fields of interest include power electronics, power quality, design of power filters and distributed power generation.

He received two national awards namely INAE Young Engineer Award from Indian National Academy of Engineering, POSOCO Power System Award from Power Grid Corporation of India in the year of 2014 for his research work. He also received Amit Garg Memorial Research Award-2014 for I.I.T Delhi for the high impact publication in a quality journal during the session 2013-2014. At present, he has published more than hundred research papers in internal national journals and conferences in field of electrical power quality.

He also serves as an Associate Editor for the IET (UK) Renewable Power Generation.

Rakesh Maurya (M'16) received B.Tech. in Electrical Engineering from the Kamla Nehru Institute of Technology Sultanpur, Uttar Pradesh in 1998 and M.Tech. and Ph.D. in Electrical Engineering from Indian Institute of Technology Roorkee, India, in 2002 and 2014 respectively. Presently, he is serving as faculty member in the Department of Electrical Engineering, Sardar Vallabhbhai National Institute of Technology Surat, Gujarat, India. His fields of interest include design of switching power converters, high power factor AC/DC converters, hybrid output converter, power quality problems, advanced electric drives and applications of real time simulator for the control of power converters.

Jayadeep Srikakolapu received the Bachelor of Technology (Electrical and Electronics) degree from JNTU, Kakinada, India, in 2010 and M.Tech. degree in Electrical Engineering with specialization in Power Electronics from SGSITS, Indore, India, in 2013. In January 2014, he joined the Department of Electrical Engineering, BVC Engineering College, Odalarevu, India, as an Assistant Professor. Since January 2018, he is doing Ph.D. program in Electrical Engineering Department from Sardar Vallabhbhai National Institute of Technology Surat, India. His research areas include power electronics, power quality and design of custom power devices and wind energy conversion systems.